Hindawi
Journal of Chemistry
Volume 2021, Article ID 5514853, 18 pages
https://doi.org/10.1155/2021/5514853

Research Article

Preparation and Characterization of Functionalized Cellulose Nanomaterials (CNMs) for Pb(II) Ions Removal from Wastewater

Hizkeal Tsade,[1] **Sisay Tadesse Anshebo**,[2] **and Fedlu Kedir Sabir**[1]

[1]*Department of Applied Chemistry, School of Applied Natural Science, Adama Science and Technology University, P.O. Box 1888, Adama, Ethiopia*
[2]*Department of Chemistry, College of Natural and Computational Science, Hawassa University, P.O. Box 05, Hawassa, Ethiopia*

Correspondence should be addressed to Hizkeal Tsade; hizts4@gmail.com

Received 3 February 2021; Revised 4 March 2021; Accepted 31 March 2021; Published 23 April 2021

Academic Editor: Ajaya Kumar Singh

Due to their remarkable properties, cellulose nanomaterials are emerging materials for wastewater (WW) treatment. In this study, both pristine cellulose nanomaterial (CNM) and sodium periodate modified cellulose nanomaterial ($NaIO_4$-CNM) were prepared from the stem of the *Erythrina brucei* plant for the removal of Pb(II) ions from WW. As-prepared CNMs were characterized by X-ray diffraction (XRD), Fourier transform infrared (FT-IR), scanning electron microscope (SEM), and thermogravimetric analysis with differential thermogravimetry (TGA-DTG) analysis. The as-prepared and characterized CNMs were tested for the removal of Pb(II) ions from secondary run-off wastewater (SERWW). Langmuir and Freundlich adsorption isotherms were certainly fixed to a maximum Pb(II) ions uptake capability (Q_{max}) of 91.74 and 384.62 mg g^{-1} by CNM and $NaIO_4$-CNM adsorbents, respectively. The pseudo-second-order (PSO) kinetics model was well fitted to the uptake process. Results revealed that the percentage removal (%R) of Pb(II) ions was decreased by the presence of nitrogen and organic matter, but not affected by the presence of phosphorous in SERWW. Due to its high efficiency, $NaIO_4$-CNM was selected for the regeneration study. The regeneration study was conducted after desorption of Pb(II) ions from the adsorbent by the addition of HCl, and the regenerated sorbent was reused as an adsorbent for at least 13 successive cycles. The results indicated excellent recycling capabilities, and the adsorbent was used as adsorbing material for the removal of Pb(II) ions from SERWW after 13 successive cycles without significant efficient loss.

1. Introduction

Water is the most important resource for all living things throughout the world [1, 2, 34]. However, water pollution is considered the greatest stimulating issue all over the world, especially in developing countries like Ethiopia [4–6]. The major sources of water pollutions are different industrial activities, urbanization, and population growth. Among these, different industries release several toxic contaminants such as heavy metals, organic dyes, pharmaceuticals, petroleum products, and others into water bodies [7–9]. Owing to their noxiousness and bioaccumulation, they provide enormous hazards to living things [10–12]. Among these pollutants, the contamination of water with heavy metals is a severe cause of environmental and human health problems [13–15]. This is because they are nonbiodegradable and can be stored in living tissues for a long time relative to organic pollutants [16, 17]. Some of these heavy metals are As, Pb, Hg, Cd, Cr, Cu, Ni, Ag, and Zn. Water bodies with high concentrations of these metals can cause severe damage to human health and aquatic animals. For instance, the presence of high concentrations of Pb in the environment causes hazardous toxicity to the reproductive systems that harms the brain, liver, and kidney of human beings and aquatic living things [18]. Furthermore, based on the toxicological studies on nephrotoxicity, exposure to Pb(II) ions can be related to renal tubular necrosis, and exposure to Pb is directly related to the failure of glomeruli [19]. As a result of this, the preparation of green and biodegradable CNMs to remove Pb(II) ions from SERWW

before its release into the different environments is very necessary [20].

Therefore, a number of technologies were tested for the removal of Pb(II) ions from wastewater, including precipitation, filtration, reverse osmosis, solvent extraction, ion exchange, coagulation, and adsorption [21]. However, most of these technologies require a high price, show low removal abilities, and require additional energy to purify wastewater [22]. From all of these, adsorption is selected because it is simple, is relatively cheap, removes pollutants at ppm levels, is highly efficient, and has abundant adsorbent materials such as activated carbon, carbon nanotubes (CNT), composites, and nanoparticles [23–25]. Among these adsorbent materials, polymeric materials such as cellulose, chitin, chitosan, gelatin, alginate, and starch have been selected currently for the removal of toxic metals from aqueous media, due to the cost-friendly and easy recycling of adsorbent materials [26].

Among these, cellulose-based materials have improved merits of being easily available, nonpoisonous, and renewable and having plenty of accessible hydroxyl functional groups which are very active for different chemical modification systems [27–31]. In spite of its pronounced properties, the demerits of cellulose-based materials in wastewater decontamination are its low hydrophilicity, physical and chemical stability, and removal capacity [32]. This shortcoming was easily improved by disintegrating cellulose into cellulose nanomaterials (CNMs) [33]. CNMs are biodegradable materials with at least one dimension in a nanometer (nm) scale. This material was prepared by disintegrating cellulose into CNMs through the addition of sulfuric acid, and the as-prepared CNMs show pronounced properties such as high surface area, small particle size, high mechanical strength, and chemical stability [34]. Depending on the preparation methods and source materials, CNMs can be classified into cellulose nanofibers (CNFs), cellulose nanocrystals (CNCs), and bacterial cellulose [35]. Among these, the study was focused on cellulose nanocrystals (CNCs) prepared from the stem of renewable and biodegradable Ethiopian indigenous *Erythrina brucei* plants.

To show the novelty of the study, the authors reviewed a number of studies that have been performed previously on the CNM-based adsorbents prepared from different polymeric materials such as sugarcane bagasse [36], date palm (*Phoenix dactylifera* L.), [37], Cotton residue [38], banana [39], corn husk [40], and *Millettia ferruginea* plant (Ethiopian indigenous plants) [41]. As per the knowledge of the authors, no work has been reported on the CNM sorbents prepared from the stem of Ethiopian indigenous *Erythrina brucei* plants (Korch in Amharic, Walensu in Afaan Oromo, Boro in Ganta). In addition, the stem of the *Erythrina brucei* plant in Ethiopia does not have significant functions and is left as waste material. Therefore, it does not influence Ethiopian economic security and is used as a low-cost adsorbent in this study. Furthermore, the majority of research reported the removal of Pb(II) ions from synthetic wastewater only, but there was a big gap found in the studies reporting the removal of Pb(II) ions from real wastewater. Therefore, this study was focused on the preparation and characterization of both CNM and NaIO4-CNM sorbent materials prepared from the stem of locally available Ethiopian indigenous *Erythrina brucei* plants for the removal of Pb(II) ions from real WW.

2. Materials and Methods

2.1. Materials and Chemicals. The stem of the *Erythrina brucei* plant was collected from Southern Region, Ganta Garo, Gamo Zone, Ethiopia, and Oromia Region, Bekoji, Arsi Zone, Ethiopia. Secondary run-off industrial wastewater (SERWW) was collected from the run of Modjo River, Modjo, Oromia Region, Ethiopia. The analytical grade chemicals and reagents used in this study, were toluene (99%, Loba Chemie Pvt. Ltd., India), ethanol (97%, Tradewell International Pvt. Ltd., India), sodium hydroxide (99%, Shraddha Associates (GUJ) Pvt. Ltd., India), conc. hydrochloric acid (35%, Loba Chemie Pvt. Ltd., India), conc. sulfuric acid (69%, Loba Chemie Pvt. Ltd., India), conc. nitric acid (69%, Loba Chemie Pvt.Ltd., India), sodium chlorite (80%, Shanghai ZZ New Material Tech. Co., Ltd., China), sodium bicarbonate (99%, Shraddha Associates (GUJ) Pvt. Ltd., India), and $Pb(NO_3)_2$ (99%, BDH Chemicals Ltd., England).

2.2. Instruments. Digital analytical balance (Explorer, Ohaus, Model E11140, Switzerland), atomic absorption spectrophotometer (AAS, Shimadzu, USA), X-ray diffraction (XRD) (XRD-7000 X-ray diffractometer, Shimadzu Co., Japan), Fourier transform infrared (FT-IR) spectroscopy (PerkinElmer 65, PerkinElmer, Inc., Waltham, USA), scanning electron microscopy (SEM) (JCM-6000Plus, JEOL/EO, USA), thermogravimetric analysis with differential thermogravimetry (TGA-DTG), a potentiometric digital pH meter (Hanna Instruments, Model MP 220, UK), conductivity meter (Model 4310), UV-VIS spectrometer (SM-spectrophotometer UV-VIS 1600, MaaLab Scientific Equipment Pvt. Ltd., India), and a water deionizer (Elga Lab Instrument, UK) were used throughout the study.

2.3. Experimental Procedures. The physicochemical property measurements of SERWW were performed and presented in Table 1. The stock solution of Pb(II) ions was prepared by taking a 1000 mL volumetric flask and adding the required amount in 1 g of $Pb(NO_3)_2$ into the flask. Then, to this flask, a certain volume of distilled water was added. The added components were carefully mixed in the form of a solution. Finally, distilled water was added up to the mark of the flask with the help of a micropipette. The diluted solutions were prepared by taking suitable volume from the previously prepared stock solution and adding it to 100 mL volumetric flasks. To these flasks, distilled water was carefully added up to the mark. Next, the physicochemical analyzed SERWW was spiked with 30 mgL^{-1} of Pb(II) ions solution and reserved for the adsorption experiments. In order to assure reproducibility, all the experiments were conducted in triplicate, and the results were reported as average values.

Table 1: Physicochemical properties of the SERWW used in the study.

Parameter	Lowest value	Maximum value	Average
pH	5.8 ± 0.03	6.3 ± 0.03	6.15 ± 0.03
EC (μS cm^{-1})	250 ± 0.5	270 ± 0.5	260 ± 0.5
COD (mg/L)	42.84 ± 0.2	63.4 ± 0.2	48.5 ± 0.2
BOD (mg/L)	35.7 ± 0.04	45.8 ± 0.04	40.75 ± 0.04
TIN (mg/L)	33.7 ± 0.02	57.8 ± 0.02	38.5 ± 0.02
NO_3^- (mg.N/L)	3.5 ± 0.04	5.9 ± 0.04	9.4 ± 0.04
NH_4^+ (mg.N/L)	36.9 ± 0.02	45.5 ± 0.02	42.3 ± 0.02
TP (mg/L)	8.9 ± 0.3	13.8 ± 0.3	10.6 ± 0.3
Mg^{2+} (mg/L)	54.2 ± 0.2	66.8 ± 0.2	60.5 ± 0.2
Cu^{2+} (mg/L)	0.26 ± 0.03	0.54 ± 0.03	0.40 ± 0.03

TP: total phosphorus, TIN: total inorganic nitrogen, BOD: biological oxygen demand, COD: chemical oxygen demand.

2.4. Preparation of Cellulose and CNMs from Erythrina brucei. The collected stem of the *Erythrina brucei* plant sample was confirmed by an Ethiopian botanist (Addis Ababa University, AAU; national herbarium). It was washed with distilled water repeatedly, dried with air at room temperature, and ground using a grinder carefully to form a coarse particle. For the extraction of CNMs, 9 g of the ground coarse particle and a 125 mL : 75 mL ratio mixture of toluene : ethanol solvent were added to a beaker and placed in a water bath for 46 hours at 50°C. Subsequently, the extracted mixture was washed with boiling water, filtrated, and dried in an oven at 50°C for 10 hours. Then, the dried fibers were cut into short fibers of approximately 5 mm in length. Next, these short fibers were treated with 100 mL of 3.0 M NaOH solution at 50°C for 2.5 hours to remove the lignin and hemicelluloses present in lignocellulosic biomass. Afterward, this mixture was washed well with deionized water repeatedly until it becomes neutral. Thereafter, the neutral mixture was centrifuged, filtered, and dried in an oven at 50°C for 10 hours. Then, the dried mixture was ground into a pulp form and bleached with a 3 : 0.75 ratio mixture by volume of sodium chlorite ($NaClO_2$) to glacial acetic acid for 4 hours at 60°C under mechanical stirring. This procedure was repeated with half of the initial amount of bleaching agent. Thereafter, it was centrifuged, washed repeatedly, and filtered, forming cellulose suspension. Subsequently, it was hydrolyzed by 100 mL of 6 M H_2SO_4 for 2 hours to break up the cell wall and to separate the fibrils present for the production of cellulose nanomaterial (CNM) suspension through sonication. Then, the prepared CNM suspension was centrifuged at 1600 rpm to separate the CNM from noncellulosic constituents and homogenized in homogenizer at 12,000 rpm for 2.0 hours. It was then washed, filtered, and dried in an oven at 50°C for 10 hours to form crystalline CNM. Finally, the prepared CNM was kept in a suitable place for characterization purposes. This procedure was adapted from Kara et al. [41] with modification, and the procedure was used throughout the experiments. The flow chart representation for the preparation of CNM is given in Figure 1.

2.4.1. Preparation of Chemically (Sodium Periodate) Modified CNM. The vicinal hydroxyl groups at carbon atoms numbers 2 and 3 in an anhydroglucose unit of cellulose were oxidized to two aldehyde groups by simultaneously breaking the carbon-carbon bond between the carbon atoms numbers 2 and 3 by using sodium periodate reagent (Figure 2). Therefore, sodium periodate is known as a specific oxidant for cellulose-based materials. Thus, 0.2 gmL^{-1} of $NaIO_4$ was dissolved into approximately 2 wt% of CNM suspension in a 250 mL flask. The flask was carefully covered with aluminum foil and stirred at 50°C in the dark for 4 hours [42]. By the addition of 1 g ethylene glycol, the excess oxidizing agents were consumed, and the reaction was completed. This procedure produces dialdehyde cellulose nanomaterial (DACNM) through centrifugation at 1600 rpm for 40 min, and it was purified by successive water addition and centrifugation. This was sonicated for 3 min at 24 kHz (Branson Digital Sonifier S-450D, South Korea). Sodium periodate cellulose nanomaterial ($NaIO_4$-CNM) was separated by centrifugation at 1600 rpm at 20°C, washed in deionized water several times until the pH of the washing medium was equal to pure water, and filtrated using filter paper no 42. Finally, the product was dried under vacuum at 50°C for 24 h. Then, it was stored in a safe place for characterization purposes.

2.5. Characterization. The crystallite size, functional groups, surface morphologies, and thermal stability of CNM and $NaIO_4$-CNM sorbents were investigated by using XRD with Cu-Kα radiation ($\lambda = 0.154$ nm) at 40 kV and 30 mA in a diffraction angle of 2θ ranging from 10° to 80° at a scan rate of 3°/min, FT-IR, SEM, and TGA-DTG analysis, respectively.

2.6. Uptake Experiments. For this experiment, the required amount of adsorbents such as CNM and $NaIO_4$-CNM and 30 mL of Pb(II) ions solutions were mixed together in 100 mL flasks. The mixture was shaken thoroughly using an orbital shaker. Subsequently, for the absorbance measurement of Pb(II) ions solutions, atomic absorption spectrophotometer (AAS, Shimadzu, USA) was used. All the uptake experiments were performed by measuring various factors that were inducing the Pb(II) ions uptake ability such as solution pH, adsorbent dose, contact time, agitation speed, and initial Pb(II) ions concentration. The effect of each parameter on the Pb(II) ions uptake ability was examined by

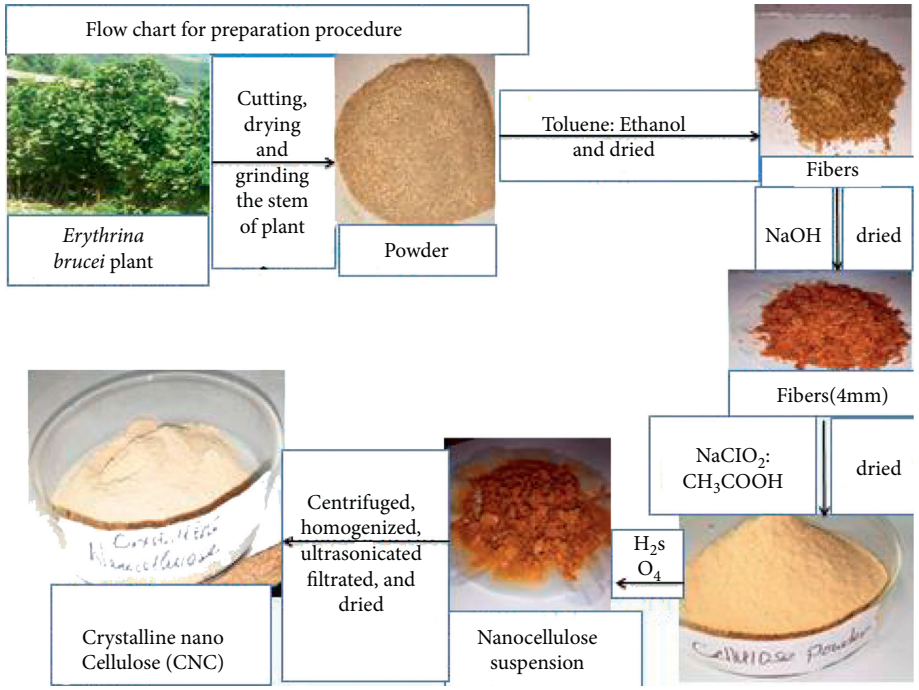

Figure 1: Flow chart representation for nanocellulose preparation from *Erythrina brucei*.

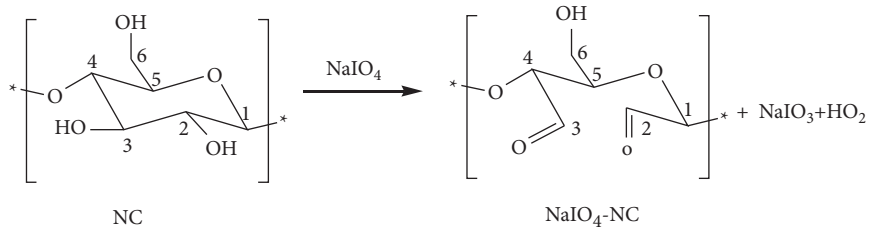

Figure 2: Sodium periodate oxidation of nanocellulose (NC).

keeping all other parameters at constant values. These parameters were determined by ranging the initial concentration of Pb(II) ions from 5 to 50 mg/L, adsorbent dosage from 0.01 to 2.5 g, contact time from 30 to 180 min, solution pH from 1 to 9, and temperature from 25 to 40°C.

2.6.1. Point of Zero Charge (pHPZC). The solution pH circumstance in which the surface charge density equals zero is termed as the pHPZC. To determine the pHPZC, the prepared adsorbents were added to 30 mL Pb(II) ions solutions with an initial pH of 2.0 to 9.0. The pH of the solution was adjusted using 0.1 M NaOH and 0.1 M HCl solutions. The suspensions were agitated on an orbital shaker at a shaking speed of 250 rpm at room temperature for 120 min. Finally, optimum pH was determined. The pHPZC was calculated using

$$\Delta pH = pH_1 - pH_2, \quad (1)$$

where pH_1 is the pH value before the experiment and pH_2 is the pH value after the experiment. In the plot of ΔpH vs pH, the intersection points at which ΔpH = 0 specify pHPZC.

2.6.2. Uptake Isotherms. Mathematically, the affinity of the Pb(II) ions uptake for CNM and $NaIO_4$-CNM adsorbent was measured using adsorption isotherms. Thus, the adsorption of Pb(II) ions by using CNM and $NaIO_4$-CNM sorbents was done using (2) and (3). From these equations, one can understand that the amount of Pb(II) ions adsorbed onto the CNM and $NaIO_4$-CNM adsorbents is equal to the amount of Pb(II) ions that were removed from the SERWW samples.

$$q_e = \frac{C_i Pb\,(\mathrm{II}) - C_e Pb\,(\mathrm{II})}{S}. \quad (2)$$

$$q_t = \frac{C_i Pb\,(\mathrm{II}) - C_t Pb\,(\mathrm{II})}{S}, \quad (3)$$

where q_e and q_t represent the amount of pollutant adsorbed onto adsorbent surfaces at equilibrium and any specified time (mgg^{-1}), respectively. $C_i Pb\,(\mathrm{II})$, $C_e Pb\,(\mathrm{II})$, and $C_t Pb\,(\mathrm{II})$ represent the initial and equilibrium concentration of $Pb\,(\mathrm{II})$ ions and concentration of $Pb\,(\mathrm{II})$ ions present in wastewater samples (mgL^{-1}) at a specified time (mgL^{-1}), respectively. S represents the slurry dosage defined as the ratio of the mass of CNM and $NaIO_4$-CNM (g) to the initial volume of the

SERWW sample (L). Initial and equilibrium concentrations were used to determine the percent Pb(II) ions removal and represented in

$$\%\text{Removal} = \frac{C_i Pb\,(\text{II}) - C_e Pb\,(\text{II})}{C_i Pb\,(\text{II})}\ x\ 100\%. \quad (4)$$

The thermodynamic study of the uptake process was conducted by investigating the basic thermodynamic parameters such as a change in Gibbs free energy (ΔG), change in enthalpy (ΔH), and change in entropy (ΔS) values [44, 45]. Therefore, in order to determine the thermal behavior of the uptake phenomenon, all predetermined and optimized values of parameters (solution pH, sorbent dosage, contact time, agitation speed, and Pb(II) ions initial concentration) were used, and the temperature was varied from 25 to 40°C.

2.6.3. Uptake Kinetics. The rate of Pb(II) ions uptake process was accomplished by using the contact times ranging from 30 to 180 min by putting all parameters such as solution pH, sorbent dose, agitation speed, and Pb(II) ions initial concentration at constant values.

2.7. Regeneration Test. From both adsorbents, $NaIO_4$-CNM was selected for sorbent regeneration study due to the higher Pb(II) ions uptake abilities, and the study was performed in removing Pb(II) ions from SERWW through replicating the laboratory work using the same $NaIO_4$-CNM sorbent for at least 13 successive cycles. Desorption of Pb(II) ions was carried out by mixing 1 g of $NaIO_4$-CNM adsorbent previously used for removing purpose with 10 mL of 0.1 M HCl solution in a 100 mL flask. Then, this mixture was stirred in an orbital shaker for 25 min. Thereafter, the $NaIO_4$-CNM sorbent was separated from the solution using centrifugation. The separated $NaIO_4$-CNM sorbent was then washed with deionized water six times, dried in the oven at room temperature, and reapplied for at least 13 successive adsorption-desorption cycles.

3. Results and Discussion

3.1. Characterization. Different characterization techniques, such as TGA-DTG, FT-IR, XRD, and SEM were tested to determine thermal stability, functional groups, crystallinity, and surface morphology, respectively, of CNM and $NaIO_4$-CNM sorbents. Specifically, the crystallinity of the sorbent materials was determined with the help of XRD spectrometry (Figure 3(a)). The XRD spectra indicated that the oxidized ($NaIO_4$-CNM) sorbent has similar peaks to the pristine CNM peaks (Figure 3(a)), and they evidently presented an amorphous nature rather than 100% crystallinity because the adsorbent materials were prepared from polymeric materials. The representative peaks at 16.16° and 22.24° for the oxidized nanocellulose ($NaIO_4$-CNM) revealed a reduced degree of crystallinity compared to the pristine CNM, as the noncompact region of the crystalline part was oxidized progressively by the reaction of $NaIO_4$ chemicals with cellulose nanomaterial suspension. Certainly, the peaks at $2\theta = 16.16°$, 22.24°, 26.6°, and 34.41° are represented by (110), (110), (200), and (004) crystallographic planes of cellulose I, respectively [46, 47]. From the XRD spectra, the crystallite particle sizes were calculated using Debye Scherrer equation (5) for both adsorbents, and the values were 2.28 nm and 2.70 nm for $NaIO_4$-CNM and CNM, respectively.

$$D_s = \frac{0.9\lambda}{\beta \cos\theta}, \quad (5)$$

where D_s is mean crystallite size (nm), λ wavelength of the incident radiation ($\lambda = 0.15405$ nm), β pure diffraction broadening (radians), and θ the Bragg angle (degrees, half-scattering angle). Usually, β is taken as the full width at half the maximum of the major diffraction band (FWHM).

The identification of functional groups and surface characteristics of the prepared CNM and $NaIO_4$-CNM sorbents was carried out by using FT-IR spectroscopy. Their spectrum was presented in Figure 3(b). The spectra have shown two major absorption zones in the ranges of 2925–3385 cm^{-1} and 611–1058 cm^{-1}. Based on these spectral zones, the CNM and $NaIO_4$-CNM sorbents have several functional groups which display either stretching vibration or bending vibration. These are (broadband around 3385 cm^{-1}) detected for both sorbents, indicating the presence of O–H free stretching vibration of the CH_2–OH structure on cellulose I [49]. The bands found in the region of 2855 cm^{-1} are because of the stretching vibration of C–H in cellulose I, and the bands situated at 1644 cm^{-1} are attributed to the O–H bending vibrations of cellulose I. The peaks detected at 1458 cm^{-1} match the C–C stretching and/or CH_2 symmetric bending in aromatic groups of cellulose I. The peaks located at 1058 cm^{-1} are associated with stretching vibration of $C = O$ groups [50]. Compared with the spectrum of pristine CNM, additional peaks were observed in oxidized cellulose nanomaterial ($NaIO_4$-CNM) at 1730 cm^{-1}, referring to the stretching vibration of the carbonyl group ($C = O$) for aldehyde due to the formation of dialdehyde cellulose nanomaterial (DACNM). These recommend that sodium periodate oxidizes the adjacent hydroxyl groups of cellulose at locations of carbon numbers 2 and 3 into aldehyde groups, simultaneously breaking the corresponding carbon-carbon bond of the glucopyranose ring in order to obtain DACNM. In addition, the increased intensity of $NaIO_4$-CNM was observed compared to CNM due to the presence of aldehyde carbonyl functional groups on the surface of $NaIO_4$-CNM. This result was in agreement with the study reported by Xiangyu et al. [51] on cationic dialdehyde nanocellulose from sugarcane bagasse for efficient chromium (VI) removal.

SEM characterization was carried out to obtain information about the surface morphology of both CNM and $NaIO_4$-CNM adsorbents. The SEM images with cylindrical rod-like shapes for both CNM and $NaIO_4$-CNM adsorbents are indicated in Figures 3(c) and 3(d). These images show that $NaIO_4$-CNM sorbent was likely to agglomerate in comparison with CNM adsorbent after drying. The addition of $NaIO_4$ to CNM suspension during the oxidation process initially degrades the amorphous regions of $NaIO_4$-CNM,

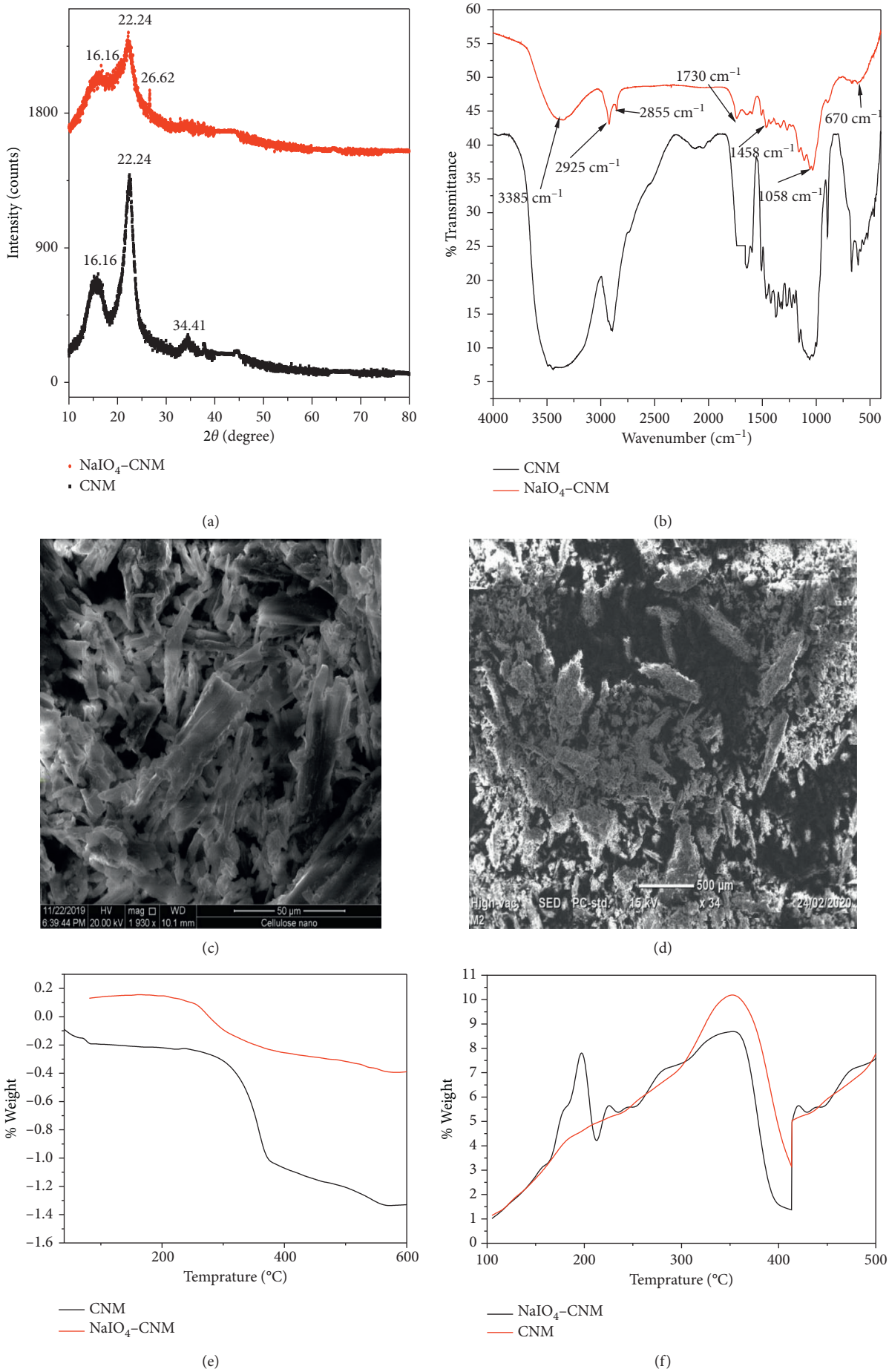

Figure 3: (a) XRD pattern, (b) FT-IR spectrum, (c, d) SEM images, and (e, f) TGA-DTG of CNM and $NaIO_4$-CNM sorbents.

and the progressive oxidation reaction takes place into the crystalline regions. Finally, aldehyde groups gained from the oxidation reaction were added to the hydroxyl groups to yield hemiacetal. These variations in biochemical arrangements also caused variations in surfaces of $NaIO_4$-CNM [52]. As a result, the rode-like structure was well observed in $NaIO_4$-CNM adsorbent after oxidation and indicated a larger specific surface area with a smaller average diameter than the pristine CNM [53].

The thermogravimetric analysis with differential thermogravimetry (TGA-DTG) behaviors of CNM and $NaIO_4$-CNM adsorbents are presented in Figures 3(e) and 3(f), respectively. Analyses of samples revealed slight weight loss at low temperature (<100°C) conforming to the vaporization of absorbed water. The TGA revealed three phases of decomposition (Figure 3(f)). Initially, 10% of mass loss was observed in the temperature range of 40–83.03°C corresponding to the dehydration and decomposition of cellulose nanomaterials. Secondly, almost 48.853% of mass loss was observed in the temperature range of 252.25–385.309°C corresponding to the scission of cellulose structure and chain, hence the discharge of CO and CO_2 and the production of carbonaceous residues [54, 55]. Thirdly, a very slow mass loss of about 14.097% was revealed after 500°C, corresponding to the decomposition of residual substances, due to the oxidation of char. Moreover, the DTG curves showed that the maximum weight loss is 411.22°C and 397.17°C for CNM and $NaIO_4$-CNM adsorbents, respectively (Figure 3(f)). In addition, the initiating temperature of degradation for $NaIO_4$-CNM was slightly lower than that of CNM, which may be expected as the periodate oxidation breaks the highly ordered bonding of crystalline CNM [56]. In general, a slight shift of $NaIO_4$-CNM curves for both TGA and DTG was possibly observed due to the presence of carbonyl functional groups on the backbone of $NaIO_4$-CNM and increased the hydrophilicity, and this provides a lower thermal decomposition temperature [57].

3.2. Physicochemical Properties of the SERWW. The experimentally measured values for the physicochemical properties of SERWW were indicated in Table 1. The pH values and electrical conductivity values were measured in different series, and the average values of 6.15 ± 0.03 and 260 ± 0.5, respectively, were reported (Table 1). From these results, it is possible to conclude that SERWW taken from near Modjo industries was nearly acidic. Besides, the chemical oxygen demand (COD), biological oxygen demand (BOD), total phosphorus (TP), total inorganic nitrogen (TIN), nitrate (NO_3^-), and (NH_4^+) values were evaluated using a replicate of trial experiments and reported as average values of 48.5 ± 0.2, 40.75 ± 0.04, 10.6 ± 0.3, 47.5 ± 0.02, 9.4 ± 0.04, and 42.3 ± 0.02, respectively. Furthermore, metals such as Mg^{2+} and Cu^{2+} ions were evaluated using a replicate of trial experiments, and their reported average values were 60.5 ± 0.2 and 0.40 ± 0.03, respectively.

3.3. Adsorption Studies

3.3.1. Effect of Initial Concentration. The effect of initial Pb(II) ions concentrations (Ci) for the removal of Pb(II) ions from SERWW using CNM and $NaIO_4$-CNM sorbent is given in Figure 4(a). At the starting point, the removal process was very fast, due to the presence of a large vacant surface area of the CNM and $NaIO_4$-CNM sorbents. At increased initial concentrations (Ci), the removal ability gradually increased, moved toward the optimum value, and reached the optimum amount of 30 mg/L. At this amount, both CNM and $NaIO_4$-CNM sorbents evidently displayed maximum Pb(II) ions uptake ability of 67.3% and 96.5%, respectively. Furthermore, a relatively higher uptake ability of Pb(II) ions was manifestly detected for $NaIO_4$-CNM sorbent than that for CNM sorbent. This is because the surface area of $NaIO_4$-CNM adsorbent was relatively increased by the surface functionalization of CNM with $NaIO_4$. Supporting this result, Chen et al. [58] reported research on As(III) removal by nanostructured dialdehyde cellulose−cysteine microscale and nanoscale fibers.

3.3.2. Effect of Contact Times. The effect of contact time on the Pb(II) ions removal was examined by using experiments at an agitation speed of 250 rpm, optimum CNM and $NaIO_4$-CNM dose of 1 g, temperature (T) of 25°C, and initial concentration of Pb(II) ions of 30 mg L^{-1} (Figure 4(b)). The %R of Pb(II) ions for both CNM and $NaIO_4$-CNM rose with raising the time up to the optimum contact time of 120 min, due to the presence of highly active sites on the surfaces of the adsorbent [59]. The maximum %R values of 72.2% and 96.8% were observed for both CNM and $NaIO_4$-CNM sorbents, respectively, at the optimum time of 120 min. After this time, the %R processes became at equilibrium and proceeded in a fixed manner. The maximum Pb(II) ions uptake abilities were detected for $NaIO_4$-CNM sorbent compared to CNM mainly because of the increased active sites of the sorbent surfaces possessing a large number of reactive aldehyde carbonyl groups and carboxylate groups.

3.3.3. Effect of Adsorbent Dose. Experiments for the %R of Pb(II) ions from the SERWW at different temperatures of 25, 30, and 40°C using CNM and $NaIO_4$-CNM adsorbent were conducted and reported at the optimum temperature of 25°C (Figure 5). During the experiment, the impact of the adsorbent dose was done by varying the amount of CNM and $NaIO_4$-CNM sorbents from 0.04 to 2.5 g, at the optimum initial concentration of 30 mg L^{-1}, agitation speed of 250 rpm, solution pH of 6, and contact time of 120 minutes. Figures 5(a) and 5(b) exhibited increased trends of Pb(II) ions %R for both CNM and $NaIO_4$-CNM sorbents initially. This trend is in agreement with research work reported by Alipour et al. [60] for Pb(II) ions removal using thiourea-functionalized magnetic ZnO/nanocellulose composite. The results also indicated that 97.8% of Pb(II) ions can be removed from wastewater by $NaIO_4$-CNM sorbent with an optimum sorbent dosage of 1 g at 25°C. Dissimilarly, 72.5% of Pb(II) ions can be removed from wastewater by CNM sorbents with an optimum sorbent dosage of 1 g at 25°C. The increased %R of Pb(II) ions by $NaIO_4$-CNM sorbent was due to the increased specific surface area resulting from the surface modification reactions. This increased specific

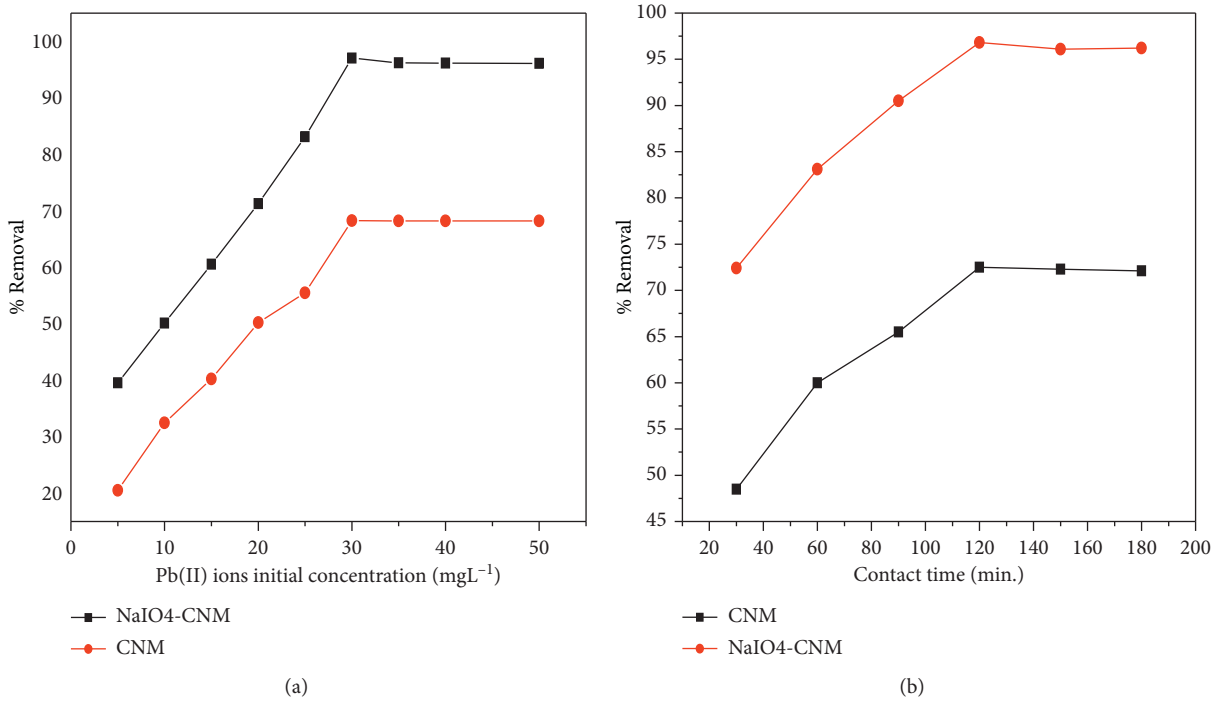

Figure 4: The effect of (a) initial concentration and (b) contact time for the removal of Pb(II) ions from wastewater, respectively, at optimum temperature of 25°C, adsorbent dosage of 1, solution pH of 6, and agitation speed of 250 rpm.

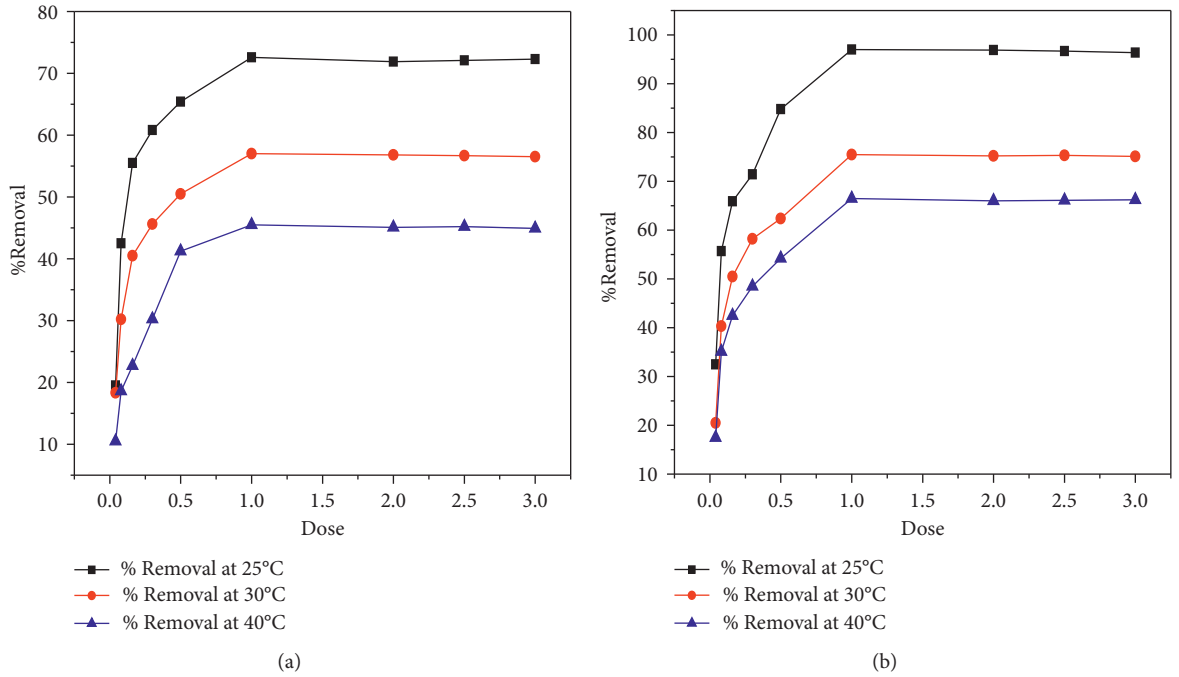

Figure 5: (a, b) The effect of adsorbent dosage at different temperatures (25, 30, and 40°C) for Pb(II) ions removal using CNM and $NaIO_4$-CNM adsorbents, respectively, at optimum contact time of 120 min, solution pH of 6, 30 mg/L initial concentration of Pb(II) ions, and agitation speed of 250 rpm.

surface area with smaller particle size resulted in a higher Pb(II) ions uptake ability since the oxidation ability of the hydroxyl groups was weaker than that of the aldehyde groups, and thus the uptake ability of CNM was lower than that of $NaIO_4$-CNM [61]. On the whole, to summarize, for both adsorbents, the %R of Pb(II) ions increased by increasing the adsorbents dosage to optimum values, and after that value the removal ability decreases. This is anticipated

because of the maximum availability of replaceable surfaces for the ions at increased concentrations of sorbents. However, at further increased concentrations there is no further increase in adsorption owing to the quantity of ions bond to the adsorbent, and the number of mobile ions in the wastewater becomes fixed even with an extra addition of the adsorbents dose [62].

3.3.4. Effect of Temperature. Figures 5(a) and 5(b) indicated the %R of Pb(II) ions from wastewater by using CNM and $NaIO_4$-CNM adsorbents. Results have shown that increasing the temperature from 25 to 40°C decreases the %R of Pb(II) ions from wastewater. Both CNM and $NaIO_4$-CNM adsorbents have shown the maximum %R (72.5% and 97.8%), respectively, of Pb(II) ions at the optimum dosage of 1 g and the optimum temperature of 25°C. This observation is in line with the reported finding that, at increased thermal behavior, the slow rate of the chemisorption processes prevents the Pb(II) ions from reaching innovative active sites on the surfaces of the adsorbents [63]. Furthermore, a much higher percentage of Pb(II) ions removal, 97.8%, was observed by using $NaIO_4$-CNM adsorbent than that using CNM adsorbent. This is due to the increased specific surface area with very small particle size obtained as a result of CNM oxidation with $NaIO_4$ [64].

3.3.5. Effect of Solution pH. The solution pH circumstance in which the surface charge density equals zero is termed as the pH point of zero charge (pHPZC). Figure 6(a) indicated the pHPZC of the material and its value was 5.0. From the plot, it is possible to deduce that the adsorbent surface is positively charged at $pH < 5.0$ and becomes negatively charged at $pH > 5.0$. Thus, for pH values < 5.0, the repulsive electrostatic force of attractions between the Pb(II) ions and positively charged functional groups of the CNM and $NaIO_4$-CNM adsorbents was dominated, and the uptake process was decreased [65]. Therefore, this recommended that higher %R of Pb(II) ions was observed at $pH > 5$ value, because, at solution $pH > 5$, the adsorbent surfaces are negative and thus react electrostatically with positively charged Pb(II) ions.

The effect of solution pH on %R of Pb(II) ions is indicated in Figure 6(b). CNM and $NaIO_4$-CNM adsorbents show high removal abilities in the solution pH range of 5–9. This is because, when the pH solution exceeds the pHPZC of the adsorbent, the surface of the adsorbent is negatively charged creating favorable conditions for Pb(II) cation uptake. This result indicated that electrostatic attraction was the main mechanism controlling the uptake of the Pb(II) ions. At low pH values, the interaction of Pb(II) ions with sorbents is decreased because of the competition of H^+ ions and other matrices for the surfaces of CNM and $NaIO_4$-CNM. In the other words, as the SERWW pH raises (i.e., less H^+ ions), the attachment of Pb(II) ions to the CNM and $NaIO_4$-CNM adsorbents leads to the increased %R at the pH value of 6. Conversely, if the pH is greater than 6, then the level of OH− ions in the SERWW increases. This phenomenon leads to the exchange of a few Pb(II) ions on the surfaces of CNM and $NaIO_4$-CNM adsorbents. Accordingly, the optimum pH for Pb(II) ions removal by both CNM and $NaIO_4$-CNM adsorbents was found to be 6. In line with this study, Olivera et al. [66] reported the maximum percent removal of Pb(II) at a pH value of 6. Supporting this view, we also made a similar report of our previous study [67]. Again, these results were in agreement with the study conducted by Qinghua et al. [68] on the uptake of Pb(II) from aqueous solutions using black wattle tannin-immobilized nanocellulose that showed increment with increasing the pH of solution form 2 to 6, and the highest adsorption capacity was observed at pH 6. At alkaline pH value, anions obtained from (HO^-) were more dominant, and the force of attraction for Pb was raised. Yeol et al. [69] showed that the increased %R of Pb(II) ions in the pH ranged from 2 to 7 using thiol-functionalized cellulose nanofiber membranes. It was reported that for $pH > 7$ the Pb(II) ions precipitate as $Pb(OH)_2$. Generally, results indicated that higher %R of Pb(II) ions was observed for $NaIO_4$-CNM adsorbents than that for CNM sorbent at a pH value of 6 (Figure 6(a)). This difference was due to the increased active sites in the surface structures of $NaIO_4$-CNM adsorbent compared to CNM adsorbent.

3.3.6. Effect of Agitation Speed. The effect of agitation speed on Pb(II) ions removal is shown in Figure 6(b). Initially, the agitation speed was slow, but as the agitation speed was increased subsequently, a rapid increase in the removal capability of Pb(II) ions was observed. This is because of the presence of fresh and smaller-sized adsorbent particles and more active sites on the binding surface of the adsorbent [70]. Thus, the removal ability of Pb(II) ions by $NaIO_4$-CNM adsorbent was increased from 73.29 to 95.72% as the agitation speed was increased from 100 to 250 rpm. In the same way, the Pb(II) ions removal ability of the CNM adsorbent was increased from 40.5 to 70.4% as the agitation speed increased from 100 to 250 rpm (Figure 6(b)). When the Pb(II) ions removal ability of the pristine CNM was compared with that of the functionalized cellulose nanomaterial ($NaIO_4$-CNM), higher removal ability was observed for $NaIO_4$-CNM due to the presence of more accessible surfaces resulting from the addition of the $NaIO_4$ to the CNM. For both adsorbents, the maximum Pb(II) ions removal capability was obtained at the optimum agitation speed of 250 rpm. This result was in agreement with the study reported by Mahmood et al. [71]. Generally, increasing the speed of agitation resulted in higher pollutant uptake abilities and helped to control the resistance of external mass transfer.

3.4. The Chemistry of SERWW. Table 2 presents a summary of the experiments carried out to determine the effects of organic matter (OM) and nutrients (N and P) on the %R of Pb(II) ions. The experiments were carried out using water samples having variable levels of COD and NOM. The water sample used in the experiments includes synthetic wastewater (SW) with initial COD level $\approx 0\ mg\ L^{-1}$, SERWW with average COD level of $48.5 \pm 0.5\ mg\ L^{-1}$, and SERWW mixed with natural organic matter (NOM) with an average COD

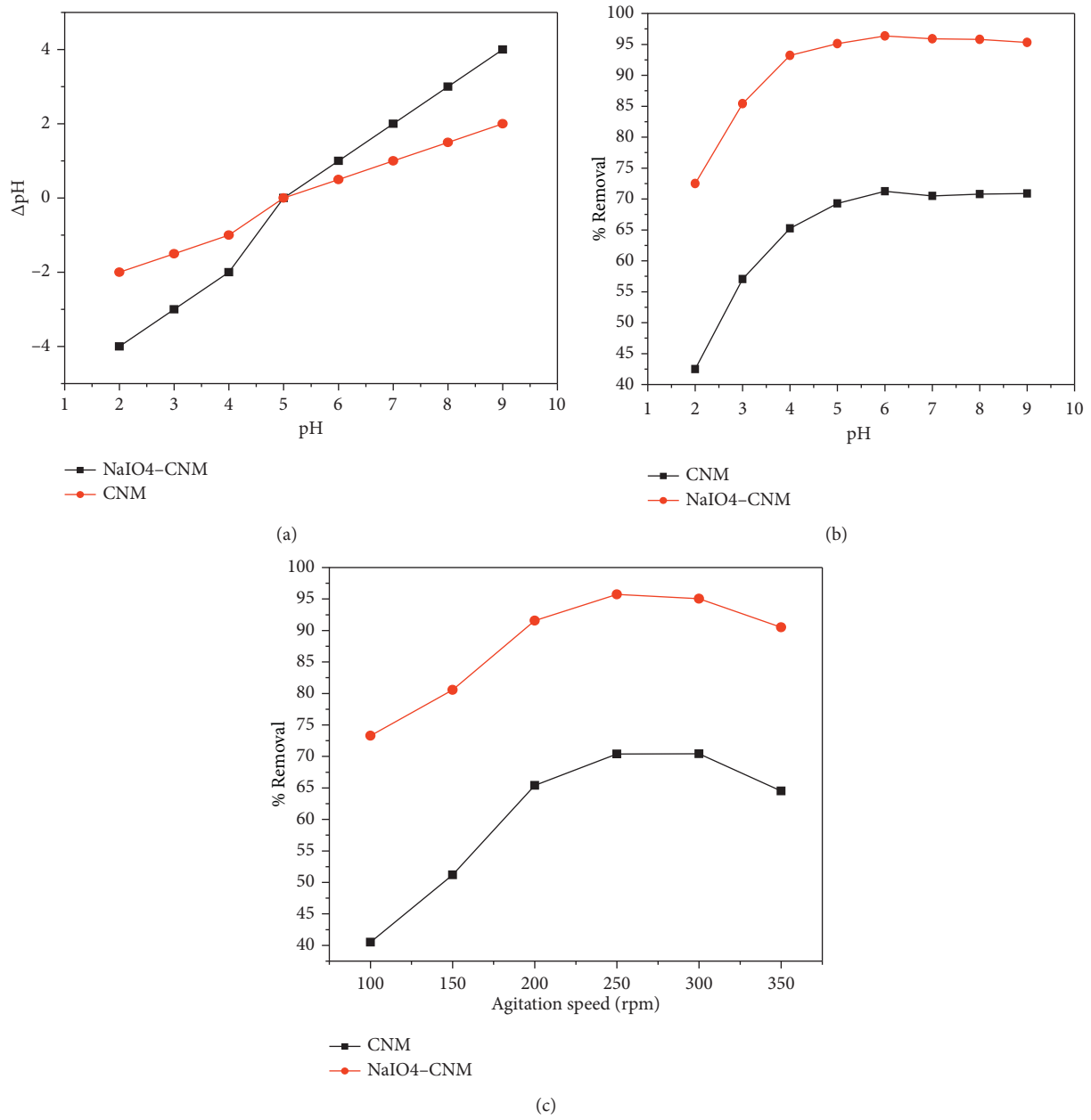

Figure 6: The consequences of (a) PZC, (b) pH, and (c) agitation speed for the removal of Pb(II) ions from wastewater at optimum initial concentration of Pb(II) ions (30 mg/L), contact time of 120 min, temperature of 25°C, and CNM and $NaIO_4$ dosage of 1 (g), respectively.

Table 2: Effect of different parameters on the Pb(II) ions removal.

Parameter	COD (mg/L)	TIN (mg/L)	TP (mg/L)	%R
SW	0	0	0	97.5
SERWW	48.5 ± 0.2	38.5 ± 0.02	6.0 ± 0.02	92.5
SERWW + NOM	104 ± 0.02	38.5 ± 0.02	6.0 ± 0.02	90.5
SW + SERWW	24.5 ± 0.01	20.2 ± 0.01	2.9 ± 0.01	94.5

level of $104.0 \pm 0.2\ mg\ L^{-1}$. Here, the SW was used as a control in the experiment because it is free of TIN, TP, and COD = 0 mg/L. The results indicated that increasing the OM level from COD ≈0 $mg\ L^{-1}$ to $104.0 \pm 0.2\ mg\ L^{-1}$ displayed a decrease in the %R of 7.0%. A decrease in the %R of Pb(II) ions by increasing the OM level resulted from the interaction between the OM and Pb(II) ions. This interaction slightly inhibits the %R of Pb(II) ions by CNM and $NaIO_4$-CNM adsorbents and decreases the %R capability of Pb(II) ions. Furthermore, the electrostatic force of attraction between the Pb(II) ions and the CNM and $NaIO_4$-CNM adsorbents is the slow step. This suggested that the electrostatic force of

attraction between the OM and the active sites on the CNM and $NaIO_4$-CNM adsorbents is restricted and does not influence the removal of Pb(II) ions from real wastewater. Therefore, it revealed that the anticipated knowledge can still be practical for contaminant removal from wastewater.

Additionally, the effect of N and P on the %R of Pb(II) ions from wastewater was determined by using the previously used water samples. Results confirmed that the Pb(II) ions uptake abilities of CNM and $NaIO_4$-CNM adsorbents were decreased by increasing the amount of nitrogen and also slightly affected by the increment of the amount of organic matter, but not affected by the increment of the amount of phosphorous and other constituents in the SERWW.

3.5. Adsorption Isotherms. To understand the mechanism of Pb(II) ions uptake by CNM and $NaIO_4$-CNM adsorbents, Langmuir (6), Freundlich (8), and Temkin (10) adsorption isotherms were investigated and presented in Figures 7(a)–7(c), respectively. Table 3 illustrates the corresponding parameter values and the correlation coefficient (R^2) values, obtained from each plot. Higher R^2 values for both Langmuir and Freundlich isotherms have shown that the Langmuir and Freundlich isotherm models better fit the isothermal uptake data than the Temkin model. This suggested that the surfaces of CNM and $NaIO_4$-CNM adsorbents were heterogeneous and physically compatible with monolayer adsorption and the adsorption process was favorable. Moreover, strong electrostatic interactions formed between the Pb(II) ions and the surfaces of adsorbents [72]. The favorability of the uptake process was due to n value that lies between 1 and 10, and the strong interactions between the adsorbates and surfaces of the adsorbents were because $1/n < 1$. The fundamental nature of the Langmuir model could be also determined by a dimensionless equilibrium parameter (RL), and its value was calculated using (7) [74]. The values (0.057 and 0.195) of $RL < 1$ suggested that the uptake process of Pb(II) ions by both CNM and NaIO4-CNM was a favorable process. Moreover, Table 3 has shown that the maximum uptake capacity of both CNM and $NaIO_4$-CNM adsorbents was 91.74 and 384.62 mg/g, respectively.where Q_{max} is the maximum uptake ability of Pb(II) ions per unit mass of adsorbent (mg g^{-1}), K_f is the uptake ability of the CNM and $NaIO_4$-CNM sorbents (mgg^{-1}), and n is the binding intensity. T is the absolute temperature in Kelvin, R is the ideal gas constant (8.314 J mol^{-1} K^{-1}), and K_C is the equilibrium constant calculated by multiplying the Pb(II) molar weight by the Langmuir constant (b).

$$\frac{C_e}{Q_e} = \frac{1}{bQ_{max}} + \frac{C_e}{Q_{max}}, \tag{6}$$

$$R_L = \frac{1}{1 + bC_0}, \tag{7}$$

$$\log qe = \log k_f + \frac{1}{n} \log Ce, \tag{8}$$

$$\Delta G^o = -RT \ln k_C, \tag{9}$$

$$Q_e = \frac{RT}{B} + \log AC_e, \tag{10}$$

The spontaneity and feasibility of the Pb(II) ions uptake process were evaluated by investigating the basic thermodynamic parameters such as a change in Gibbs free energy (ΔG), change in enthalpy (ΔH), and change in entropy (ΔS) values. Results have shown that the calculated ΔG ($kJmol^{-1}$) value presented in Table 3 was negative and confirmed that the Pb(II) ions uptake mechanism was spontaneous and feasible.

3.6. Adsorption Kinetics. In order to investigate the rates of uptake mechanism, pseudo-first-order (PFO), pseudo-second-order (PSO), and intraparticle diffusion kinetic models were tested. For these, the rates of Pb(II) ions uptake by CNM and $NaIO_4$-CNM sorbents were estimated using linearized pseudo-first-order (PFO) (11), pseudo-second-order (PSO) (12), and intraparticle diffusion (13), respectively.

$$\log (qe - qt) = \log qe - \frac{K_1 t}{2.303}, \tag{11}$$

$$\frac{t}{q_t} = \frac{1}{K_2 q_e^2} + \frac{t}{q_e}, \tag{12}$$

$$Q_t = k_p t^{0.5} + C_i. \tag{13}$$

The kinetics data are presented in Table 4 with maximum correlation coefficient values ($R^2 = 0.965$ and 0.970, for PSO) and unsatisfactory correlation coefficient values ($R^2 = 0.576$, 0.837, 0.703, 0.542 for PFO and interparticle diffusion model) by CNM and $NaIO_4$-CNM sorbents for Pb(II) ions uptake, respectively. Thus, R^2 values indicated that PFO and intraparticle diffusion kinetic models were too poor and not suitable for Pb(II) ions adsorption. Therefore, Figures 8(a) and 8(b)) indicate representative fitness of the data for PSO for Pb(II) ions uptake by CNM and $NaIO_4$-CNM sorbents and suggest that the uptake process is chemisorption. Moreover, to support this view, the application of Root Mean Square Error (RMSE) calculations for the statistical evaluation of data is very important. Thus, the RMSE values for CNM and NaIO4-CNM adsorbents were 0.493 and 0.013, respectively, given in Table 4. From these values, it is possible to conclude that the calculated value and experimental value were closer to each other and confirm a representative fitness of the data for PSO for Pb(II) ions uptake by CNM and $NaIO_4$-CNM sorbents.

3.7. Adsorption Mechanism. The probable mechanism of Pb(II) ions uptake by CNMs is schematically represented in Figure 9. From the figure, it could be inferred that the hydroxyl, carbonyl, and carboxyl groups are mainly responsible for the uptake of Pb(II) ions: Pb^{2+} (aq) + R(OH,CO,COOH) ⟶ $Pb(R(OH,CO,COOH))^{2+}$.

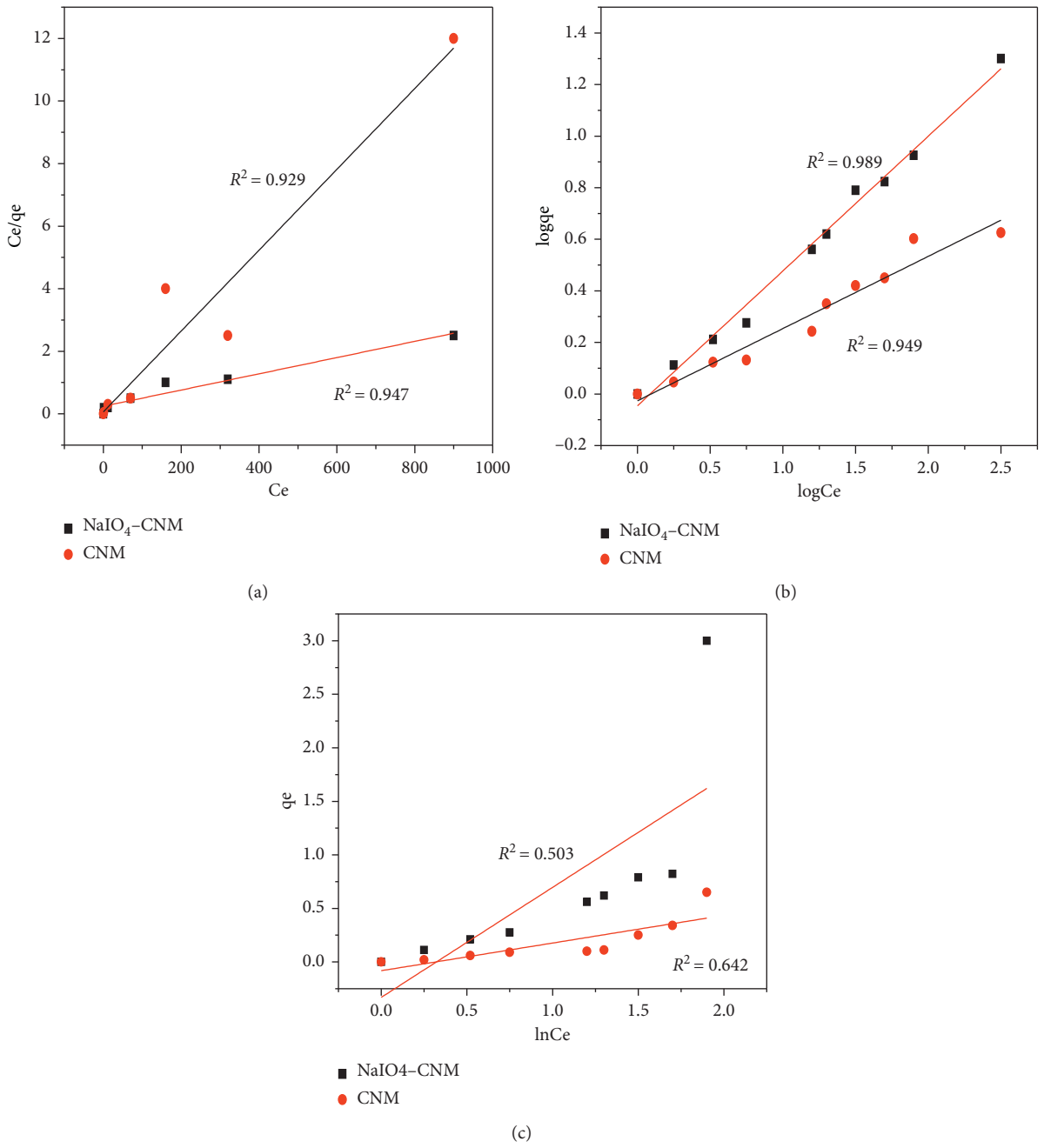

Figure 7: Langmuir (a), Freundlich (b), and Temkin (c) adsorption isotherm for the removal of Pb(II) ions, respectively, at Ci = 30 mg/L, pH = 6, adsorbent dose = 1 (g), contact time = 120 min, and agitation speed = 250 rpm.

Table 3: Langmuir, Freundlich, and Temkin isotherm constants for Pb(II) ions adsorption by CNC and NaIO$_4$-CNM sorbent at 25°C.

Isotherm models	Langmuir				Freundlich				Temkin		
	Q_{max} (mg/g)	b	R_L	R^2	K_f (mg/g)	n	R^2	ΔG° (kJmol^{-1})	K_T	B	R^2
CNM	91.74	0.18	0.057	0.929	0.94	3.57	0.949	−2.244	3.71	9225	0.703
NaIO$_4$-CNM	384.62	0.011	0.195	0.947	0.899	1.91	0.989	−4.47	0. 46	232.9	0.542

Table 4: The values of parameters and correlation coefficients of pseudo-first-order (PFO), pseudo-second-order (PSO), and intraparticle diffusion kinetic models.

Kinetics	PFO				PSO					Interparticle diffusion		
	q_e. cal. (mg/g)	q_e. exp. (mg/g)	K_1	R^2	q_e. cal. (mg/g)	q_e. exp. (mg/g)	K_2	R^2	RMSE	K_p	Ci	R^2
CNM	1.220	89.78	0.173	0.576	88.49	89.78	0.003	0.965	0.493	0.247	−0.200	0.703
$NaIO_4$-CNM	1.315	271.5	0.380	0.837	270.27	271.5	0.0015	0.941	0.013	0.043	−0.048	0.542

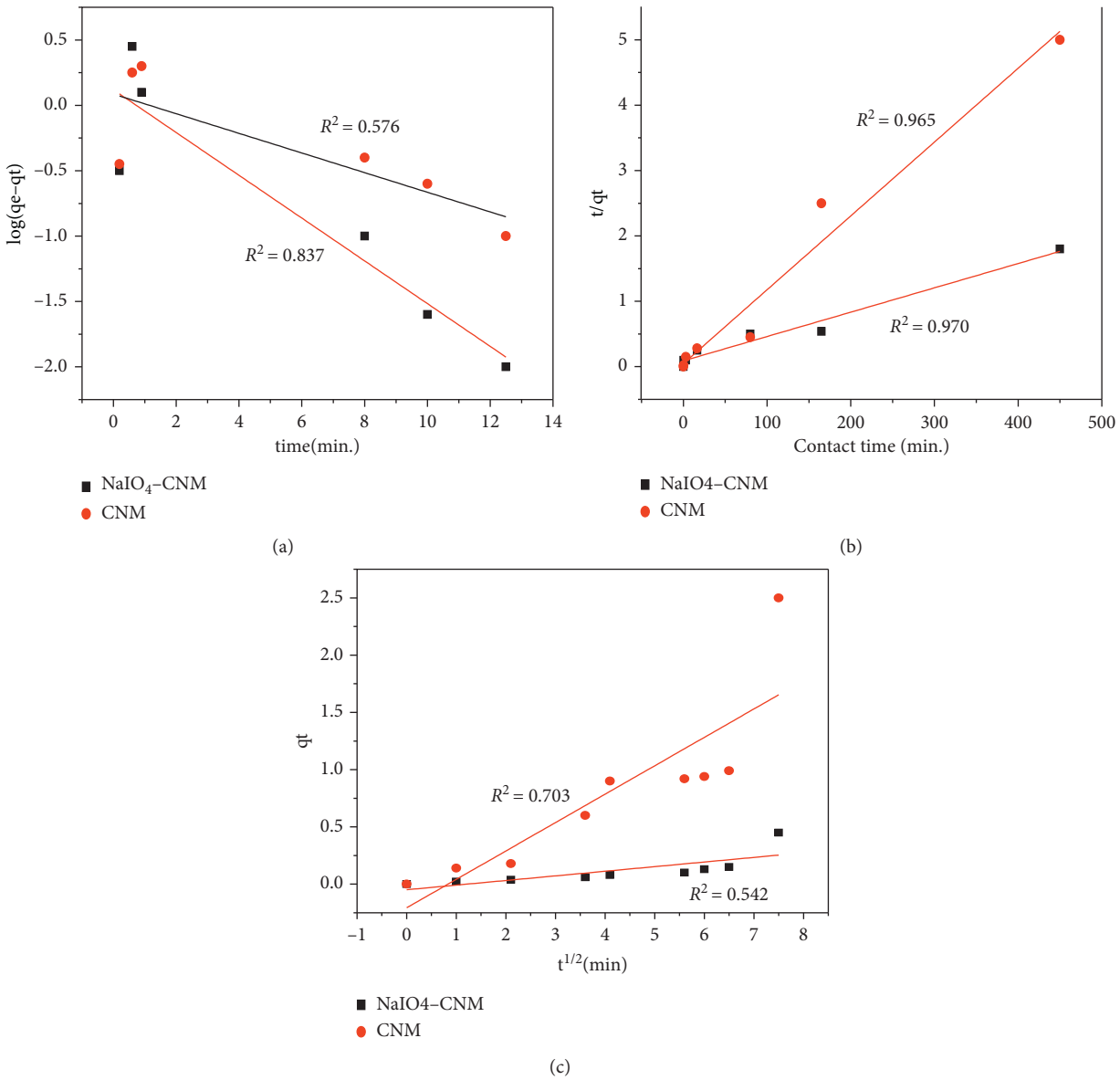

Figure 8: Plot of the PFO (a), PSO (b), and intraparticle diffusion (c) model at Co = 30 mg/L, pH = 6, adsorbent dose = 1 (g), contact time = 120 min, and agitation speed = 250 rpm for Pb(II) ions and Ni(II) ions removal, respectively.

This adsorption mechanism was performed via electrostatic interactions between the Pb(II) ions and the hydroxyl, carbonyl, and carboxyl groups, and chemical activity of these functional groups on the surface of CNMs contributes to the uptake process.

3.8. Comparison with Other Adsorbents. Table 5 represents the comparative results reported for Pb(II) ions removal by other adsorbents. The maximum Pb(II) ions uptake (Q_{max}) values of the CNM and $NaIO_4$-CNM were 91.74 and 384.62 mgg^{-1}, respectively, using the Langmuir adsorption

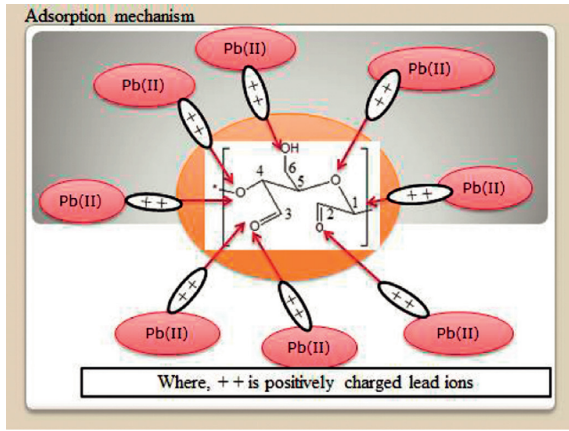

Figure 9: Adsorption mechanism of Pb(II) ions removal by CNMs.

Table 5: Comparison of adsorption capacity of Pb(II) ions by different adsorbents.

Adsorbent	Adsorption condition	Q_{max} (mg/g)	Isotherms	Kinetics	References
Chitosan functionalized with xanthate	25°C, pH 4	322.6	Langmuir	PSO	[81]
Tannin-nanocellulose (TNCC)	25°C, pH 6	53.37	Langmuir	PSO	[82]
Activated carbon	25°C, pH 7	47.61	Langmuir	PSO	[83]
Fe_3O_4@TATS@ATA	25°C, pH 5.7	205.2	Langmuir	PSO	[84]
CYCS/CNC	25°C, pH 7	334.9	Langmuir	PSO	[85]
Magnetic hydrogel beads (m-CS/PVA/CCNFs)	35°C, pH 4.5	171	Langmuir	PSO	[86]
Biomass-magnetic hybrid	25°C, pH 6.8	63.6	Langmuir	PSO	[87]
CNM	25°C, pH 6.0	91.74	Langmuir	PSO	This work
$NaIO_4$-CNM	25°C, pH 6.0	384.62	Langmuir	PSO	This work

isotherm model. As can be observed in Table 5, the uptake capacity of both adsorbents in this study is higher than that of the majority of the adsorbents reported in the literature [81–87]. Furthermore, the uptake of Pb(II) ions by tannin-nanocellulose (TNCC) at the same pH of 6 has lower uptake capacity than the present adsorbents Pb(II) ions uptake capacity. This approves the possibility of using CNM and $NaIO_4$-CNM adsorbents with cost effectiveness, in comparison to other previously used adsorbents. Because of their simplicity, nontoxicity, cost effectiveness, and biodegradability, CNM and $NaIO_4$-CNM adsorbents have great potential for effective removal of Pb(II) ions from real WW.

3.9. Regeneration Test. Because of its exceptional uptake ability as sorbent material, $NaIO_4$-CNM was carefully chosen for recycling experiments. The desorption and regeneration experimental procedures were done by evaluating the %R of Pb(II) ions after the 1st, 4th, and 13th cycles and presented in Figure 10. The purpose of regeneration experiments was to make a cost-friendly contaminant uptake process from wastewater. This was done by using desorption experiments. Desorption of Pb(II) ions from the sorbents was performed with the help of HCl solution. The regenerated sorbent was reused for at least 13 cycles, and it was shown that the uptake ability of Pb(II) ions for $NaIO_4$-CNM sorbent progressively decreased with increasing the cycles of reusable trial. The decrease in uptake ability of the sorbent with increased frequency of reusability times is normal, because of the loss of active sites on the $NaIO_4$-

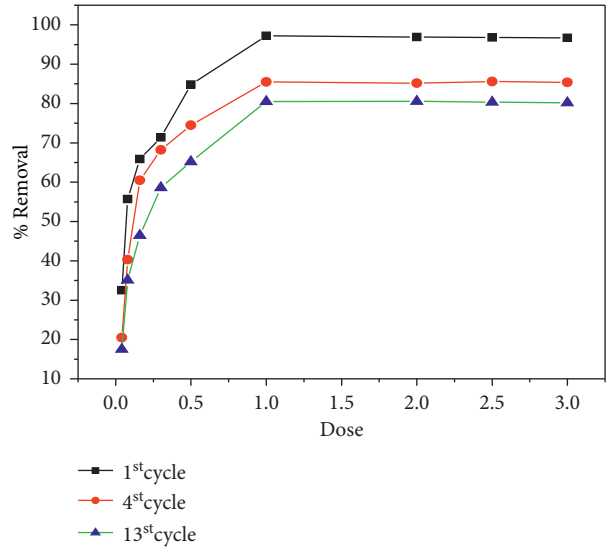

Figure 10: Percentage of Pb(II) ions removal after different cycles (1st, 4th, and 13th) by $NaIO_4$-CNM sorbent.

CNM sorbent [88]. However, it was found that the uptake ability of the $NaIO_4$-CNM sorbent did not meaningfully change after the 13th cycle of the procedure as the %R was up to that point advanced. The results have shown that the %R for the 13 consecutive cycles was decreased below 5.5%. From this result, it is possible to conclude that $NaIO_4$-CNM sorbent can be used for contaminant uptake for a long time with an exceptional possibility. The results were in

agreement with the review study conducted by Chang et al. and Chu et al. [89, 90] on the removal of heavy metals from wastewater by using molybdenum disulfide sorbent.

4. Conclusion

Biodegradable and biocompatible pristine and chemically modified cellulose nanomaterials were prepared by sulfuric acid hydrolysis methods. The as-prepared adsorbent materials were employed as cost-effective, easily recyclable, and nontoxic materials, with high uptake abilities, for the uptake of Pb(II) ions from real wastewater. The proposed mechanisms for the uptake process under the optimum circumstance of $NaIO_4$-CNM adsorbent mainly involve the interaction of ester, carboxyl, and hydroxyl groups of cellulose with Pb(II) ions that resulted in higher Pb(II) ions uptake ability for the functionalized adsorbent than the pristine one. The uptake mechanism fits with Langmuir and Freundlich uptake isotherm models, and the kinetics of Pb(II) ions uptake by CNM and $NaIO_4$-CNM adsorbents were described with the help of the PSO kinetics model. Both CNM and $NaIO_4$-CNM adsorbents showed the maximum adsorption capacity of 91.74 and 384.62 mgL^{-1} at an optimum pH value of 6. For the regeneration study, $NaIO_4$-CNM adsorbent was selected because of its high uptake ability, and the results of regeneration experiment have proven that it was recyclable and economically friendly material reused for different successive cycles. From this point, one can conclude that $NaIO_4$-CNM adsorbent proved to be a cost-effective and environmentally friendly adsorbent for the uptake of Pb(II) ions from wastewater.

Data Availability

The data used to support the results of this study are included within the article.

Conflicts of Interest

The authors declare no potential conflicts of interest with respect to the research, authorship, and/or publication of this manuscript.

Acknowledgments

The authors acknowledge Adama Science and Technology University for providing the funds and accommodations required for doing this work. This work has been funded by Project no. SoANS/JV-259298/2019, Research and Technology Transfer Office, Adama Science and Technology University (ASTU).

References

[1] E. Berger, P. Haase, M. Kuemmerlen, M. Leps, R. B. Schäfer, and A. Sundermann, "Water quality variables and pollution sources shaping stream macroinvertebrate communities," *Science of the Total Environment*, vol. 588, pp. 1–10, 2017.

[2] R. Brandes, D. Belosinschi, F. Brouillette, and B. Chabot, "A new electrospun chitosan/phosphorylated nanocellulose biosorbent for the removal of cadmium ions from aqueous solutions," *Journal of Environmental Chemical Engineering*, vol. 7, no. 6, Article ID 103477, 2019.

[3] N. B. Thi Tran, N. B. Duong, and N. L. Le, "Synthesis and characterization of magnetic Fe3O4/zeolite NaA nanocomposite for the adsorption removal of methylene blue potential in wastewater treatment," *Journal of Chemistry*, vol. 2021, Article ID 6678588, 10 pages, 2021.

[4] S. M. Anush, H. R. Chandan, and B. Vishalakshi, "Synthesis and metal ion adsorption characteristics of graphene oxide incorporated chitosan Schiff base," *International Journal of Biological Macromolecules*, vol. 126, pp. 908–916, 2019.

[5] C. E. Jackcina Stobel, G. Sreerag, A. Rajeswari, G. Sudharsan, and P. Anitha, "Highly crosslinked 3-D hydrogels based on graphene oxide for enhanced remediation of multi contaminant wastewater," *Journal of Water Process Engineering*, vol. 31, Article ID 100850, 2019.

[6] M. A. Tofighy and T. Mohammadi, "Divalent heavy metal ions removal from contaminated water using positively charged membrane prepared from a new carbon nanomaterial and HPEI," *Chemical Engineering Journal*, vol. 388, pp. 124–192, 2020.

[7] S. Hokkanen, A. Bhatnagar, and M. Sillanpää, "A review on modification methods to cellulose-based adsorbents to improve adsorption capacity," *Water Research*, vol. 91, pp. 156–173, 2016.

[8] A. Mohd, W. Aini, W. Ibrahim et al., "New effective 3-aminopropyltrimethoxysilane functionalized magnetic sporopollenin-based silica coated graphene oxide adsorbent for removal of Pb (II) from aqueous environment," *Journal of Environmental Management*, vol. 253, Article ID 109658, 2020.

[9] X. Qin, L. Bai, Y. Tan, L. Li, F. Song, and Y. Wang, "β-Cyclodextrin-crosslinked polymeric adsorbent for simultaneous removal and stepwise recovery of organic dyes and heavy metal ions: fabrication, performance and mechanisms," *Chemical Engineering Journal*, vol. 372, pp. 1007–1018, 2019.

[10] A. Md Ariful, R. P. S. Alain, N. N. Aruna et al., "Metal-Organic frameworks-derived multifunctional carbon encapsulated metallic nanocatalysts for catalytic peroxymonosulfate activation and electrochemical hydrogen generation," *Molecular Catalyst*, vol. 498, Article ID 111241, 2020.

[11] C. He, Z. Yang, J. Ding, Y. Chen, X. Tong, and Y. Li, "Effective removal of Cr(VI) from aqueous solution by 3-aminopropyltriethoxysilane-functionalized graphene oxide," *Colloids and Surfaces A: Physicochemical and Engineering Aspects*, vol. 520, pp. 448–458, 2017.

[12] A. Amanda, A. Rifathin, A. Arum, and Y. Sampora, "Oil palm empty fruit bunch-based nanocellulose as a super-adsorbent for water remediation," *Carbohydrate Polymer*, vol. 229, Article ID 115433, 2020.

[13] T. Shahnaz, V. Sharma, S. Subbiah, and S. Narayanasamy, "Multivariate optimisation of Cr (VI), Co (III) and Cu (II) adsorption onto nanobentonite incorporated nanocellulose/chitosan aerogel using response surface methodology," *Journal of Water Process Engineering*, vol. 36, Article ID 101283, 2020.

[14] A. Tshikovhi, S. B. Mishra, and A. K. Mishra, "Nanocellulose-based composites for the removal of contaminants from wastewater," *International Journal of Biological Macromolecules*, vol. 152, pp. 616–632, 2020.

[15] G. Bhanjana, N. Dilbaghi, K.-H. Kim, and S. Kumar, "Carbon nanotubes as sorbent material for removal of cadmium," *Journal of Molecular Liquids*, vol. 242, pp. 966–970, 2017.

[16] K. Atkovska, K. Lisichkov, G. Ruseska, A. T. Dimitrov, and A. Grozdanov, "Removal of heavy metal ions from wastewater using conventional and nanosorbents: a review," *Journal of Chemical Technology Metall*, vol. 53, no. 2, pp. 202–219, 2018.

[17] K. Nguyen, B. Nguyen, H. Nguyen, and H. Nguyen, "Adsorption of arsenic and heavy metals from solutions by unmodified iron-ore sludge," *Applied Sciences*, vol. 9, no. 4, p. 619, 2019.

[18] Q. Xu, Y. Wang, L. Jin, and Y. Wang, "Adsorption of Cu (II), Pb (II) and Cr (VI) from aqueous solutions using black wattle tannin-immobilize," *Journal of Hazardous Materials*, vol. 340, pp. 91–99, 2018.

[19] R. A. S. D. Rathnasekara, W. S. M. Botheju, J. A. Liyanage, S. K. Weragoda, and K. A. M. Kularathne, "Risk assessment of trace element contamination in drinking water and agricultural Soil : a study in selected chronic kidney disease of unknown etiology (CKDu) endemic areas in Sri Lanka," *Journal of Chemistry*, vol. 2021, Article ID 6627254, 10 pages, 2021.

[20] A. Mautner, Y. Kwaw, K. Weiland et al., "Natural fibre-nanocellulose composite filters for the removal of heavy metal ions from water," *Industrial Crops and Products*, vol. 133, pp. 325–332, 2019.

[21] J. Li, K. Zuo, W. Wu et al., "hape memory aerogels from nanocellulose and polyethyleneimine as a novel adsorbent for removal of Cu (II) and Pb (II)," *Carbohydrate Polymers*, vol. 196, pp. 376–384, 2018.

[22] S. Hokkanen, A. Bhatnagar, V. Srivastava, V. Suorsa, and M. Sillanpää, "Removal of Cd2+, Ni2+ and PO43− from aqueous solution by hydroxyapatite-bentonite clay-nanocellulose composite," *International Journal of Biological Macromolecules*, vol. 118, pp. 903–912, 2018.

[23] M. Abdulfeta, T. Biruktawit, H. Abdulrazak, A. Bedasa, K. Fedlu, and E. " Rajalakshmanan, "Activated carbon adsorbent derived from *Erythrina brucei* stem powder on industrial waste water treatment," *International Journal of Scientific Engineering Research*, vol. 8, pp. 1427–1432, 2019.

[24] B. Gaurav, D. Neeraj, K. Ki-Hyun, and K. Sandeep, "Carbon nanotubes as sorbent material for removal of cadmium," *Journal of Molecular Liquid*, vol. 242, 2017.

[25] J. Li, K. Zuo, W. Wu et al., "Shape memory aerogels from nanocellulose and polyethyleneimine as a novel adsorbent for removal of Cu(II) and Pb(II)," *Carbohydrate Polymers*, vol. 196, pp. 376–384, 2018.

[26] K. Pyrzynska, "Removal of cadmium from wastewaters with low-cost adsorbents," *Journal of Environmental Chemical Engineering*, vol. 7, no. 1, Article ID 102795, 2019.

[27] A. Md Ariful, A. I. Muhammad, R. P. S. Alain et al., "N Juan "Spent tea leaves templated synthesis of highly active and durable cobalt-based trifunctional versatile electrocatalysts for hydrogen and oxygen evolution and oxygen reduction reactions," *Green Chemistry*, vol. 22, pp. 6967–6980, 2021.

[28] D. Noemi, T. Brenda, A. B. Luis et al., "Bimetallic CoMoS composite anchored to biocarbon fibers as a high-capacity anode for Li-ion batteries," *ACS Omega*, vol. 3, pp. 10243–10249, 2018.

[29] M. Ghanbarian, R. Nabizadeh, S. Nasseri et al., "Potential of amino-riched nano-structured MnFe2O4@cellulose for biosorption of toxic Cr (VI): modeling, kinetic, equilibrium and comparing studies," *International Journal of Biological Macromolecules*, vol. 104, pp. 465–480, 2017.

[30] V. Kumar, S. Latha, T. Gomathi, and P. N. Sudha, "Batch adsorption and desorption studies on the removal of lead (II) from aqueous solution using nanochitosan/sodium alginate/microcrystalline cellulose beads," *International Journal of Biological Macromolecules*, vol. 104, 2017.

[31] F. Yazdi, M. Anbia, and S. Salehi, "Characterization of functionalized chitosan-clinoptilolite nanocomposites for nitrate removal from aqueous media," *International Journal of Biological Macromolecules*, vol. 130, pp. 545–555, 2019.

[32] T. S. Anirudhan and F. Shainy, "Effective removal of mercury(II) ions from chlor-alkali industrial wastewater using 2-mercaptobenzamide modified itaconic acid-grafted-magnetite nanocellulose composite," *Journal of Colloid and Interface Science*, vol. 456, pp. 22–31, 2015.

[33] T. S. Anirudhan, J. R. Deepa, and J. Christa, "Nanocellulose/nanobentonite composite anchored with multi-carboxyl functional groups as an adsorbent for the effective removal of Cobalt(II) from nuclear industry wastewater samples," *Journal of Colloid and Interface Science*, vol. 467, pp. 307–320, 2016.

[34] K. Gupta, A. Kaushik, K. B. Tikoo et al., "Enhanced catalytic activity of composites of $NiFe_2O_4$ and nano cellulose derived from waste biomass for the mitigation of organic pollutants," *Arabian Journal of Chemistry*, vol. 13, no. 1, pp. 783–798, 2017.

[35] H.-M. Ng, L. T. Sin, T.-T. Tee et al., "Extraction of cellulose nanocrystals from plant sources for application as reinforcing agent in polymers," *Composites Part B: Engineering*, vol. 75, pp. 176–200, 2015.

[36] R. Z. Khoo, W. S. Chow, and H. Ismail, "Sugarcane bagasse fiber and its cellulose nanocrystals for polymer reinforcement and heavy metal adsorbent: a review," *Cellulose*, vol. 25, no. 8, pp. 4303–4330, 2018.

[37] A. Adel, A. El-Shafei, A. Ibrahim, and M. Al-Shemy, "Extraction of oxidized nanocellulose from date palm (*Phoenix Dactylifera L.*) sheath fibers: influence of CI and CII polymorphs on the properties of chitosan/bionanocomposite films," *Industrial Crops and Products*, vol. 124, pp. 155–165, 2018.

[38] J. H. O. Do Nascimento, R. F. Luz, F. M. F. Galvao et al., "Extraction and characterization of cellulosic nanowhisker obtained from discarded Cotton fibers," *Materials Today: Proceedings*, vol. 2, no. 1, pp. 1–7, 2015.

[39] K. Harini, K. Ramya, and M. Sukumar, "Extraction of nano cellulose fibers from the banana peel and bract for production of acetyl and lauroyl cellulose," *Carbohydrate Polymers*, vol. 201, pp. 329–339, 2018.

[40] X. Yang, F. Han, C. Xu et al., "Effects of preparation methods on the morphology and properties of nanocellulose (NC) extracted from corn husk," *Industrial Crops and Products*, vol. 109, pp. 241–247, 2017.

[41] H. T. Kara, S. T. Anshebo, and F. K. Sabir, "A novel modified cellulose nanomaterials (CNMs) for remediation of chromium (VI) ions from wastewater," *Materials Research Express*, vol. 7, no. 11, Article ID 115008, 2020.

[42] X. Xu, Y. Long, Q. Li et al., "Modified cellulose membrane with good durability for effective oil-in-water emulsion treatment," *Journal of Cleaner Production*, vol. 211, pp. 1463–1470, 2019.

[43] J. Chen, H. Kong, D. Wu, X. Chen, D. Zhang, and Z. Sun, "Phosphate immobilization from aqueous solution by fly ashes in relation to their composition," *Journal of Hazardous Materials*, vol. 139, no. 2, pp. 293–300, 2007.

[44] E. I. Unuabonah, K. O. Adebowale, and B. I. Olu-Owolabi, "Kinetic and thermodynamic studies of the adsorption of lead (II) ions onto phosphate-modified kaolinite clay," *Journal of Hazardious Materials*, vol. 144, no. 1-2, pp. 386–395, 2007.

[45] L. Segal, J. J. Creely, and A. E. Martin, "An empirical method for estimating the degree of crystallinity of native cellulose using the X-ray diffractometer," *Text Research Journal*, vol. 4, 1959.

[46] D. Wei, Q. Liu, Z. Liu et al., "Modified nano microfibrillated cellulose/carboxymethyl chitosan composite hydrogel with giant network structure and quick gelation formability," *International Journal of Biological Macromolecules*, vol. 135, pp. 561–568, 2019.

[47] Z. Xiang, W. Gao, L. Chen, W. Lan, and J. Y. Runge, "A comparison of cellulose nanofibrils produced from Cladophora glomerata algae and bleached eucalyptus pulp," *Cellulose*, vol. 23, no. 1, pp. 493–503, 2016.

[48] I. Ahmad and A. Dufresne, "Effects of hydrolysis conditions on the morphology. crystallinity, and thermal stability of cellulose nanocrystals," *Cellulose*, vol. 19, no. 3, pp. 855–866, 2012.

[49] X. Huang, G. Dognani, P. Hadi, M. Yang, A. E. Job, and B. S. Hsiao, "Cationic dialdehyde nanocellulose from sugarcane bagasse for efficient chromium(VI) removal," *ACS Sustainable Chemistry & Engineering*, vol. 8, no. 12, pp. 4734–4744, 2020.

[50] D. J. Mendoza, C. Browne, V. S. Raghuwanshi, G. P. Simon, and G. Garnier, "One-shot TEMPO-periodate oxidation of native cellulose," *Carbohydrate Polymers*, vol. 226, p. 115292, 2019.

[51] W. Li, B. Ju, and S. Zhang, "Novel amphiphilic cellulose nanocrystals for pH-responsive Pickering emulsions," *Carbohydrate Polymers*, vol. 229, Article ID 115401, 2020.

[52] Y. Tang, S. Yang, N. Zhang, and J. Zhang, "Preparation and characterization of nanocrystalline cellulose via low-intensity ultrasonic-assisted sulfuric acid hydrolysis," *Cellulose*, vol. 21, no. 1, pp. 335–346, 2014.

[53] J. Lindh, D. O. Carlsson, M. Stromme, and A. Mihranyan, "Convenient one-pot formation of 2,3-dialdehyde cellulose beads via periodate oxidation of cellulose in water," *Biomacromolecule*, vol. 15, no. 5, pp. 1928–1932, 2014.

[54] R. Chang-Qing, S. Maria, and L. Jonas, "Preparation of porous 2,3-dialdehyde cellulose beads crosslinked with chitosan and their application in adsorption of Congo red dye," *Carbohydrate Polymer*, vol. 181, pp. 200–207, 2018.

[55] T. S. Anirudhan and T. A. Rauf, "Adsorption performance of amine functionalized cellulose grafted epichlorohydrin for the removal of nitrate from aqueous solutions," *Journal of Industrial and Engineering Chemistry*, vol. 19, no. 5, pp. 1659–1667, 2013.

[56] H. Chen, S. K. Sharma, P. R. Sharma, H. Yeh, K. Johnson, and B. S. Hsiao, "Arsenic(III) "removal by nanostructured dialdehyde Cellulose–Cysteine microscale and nanoscale fibers," *ACS Omega*, vol. 42, pp. 2008–22020, 2019.

[57] X. Ma, M. Lv, D. P. Anderson, and P. R. Chang, "Natural polysaccharide composites based on modified cellulose spheres and plasticized chitosan matrix," *Food Hydrocolloids*, vol. 66, pp. 276–285, 2017.

[58] A. Alipour, S. Zarinabadi, A. Azimi, and M. Mirzaei, "Adsorptive removal of Pb(II) ions from aqueous solutions by thiourea-functionalized magnetic ZnO/nanocellulose composite: optimization by response surface methodology (RSM)," *International Journal of Biological Macromolecules*, vol. 151, pp. 124–135, 2020.

[59] L. Dai, Y. Wang, Z. Li et al., "A multifunctional self-crosslinked chitosan / cationic guar gum composite hydrogel and its versatile uses in phosphate-containing water treatment and energy storage," *Carbohydrate Polymers*, vol. 244, pp. 116–472, 2020.

[60] B. H. Hameed, U. G. Akpan, and K. P. Wee, "Photocatalytic degradation of Acid Red 1 dye using ZnO catalyst in the presence and absence of silver," *Desalination and Water Treatment*, vol. 27, no. 3, pp. 204–209, 2011.

[61] A. Radhakrishnan, J. Nahi, and B. Beena, "Synthesis and characterization of multi-carboxyl functionalized nanocellulose/graphene oxide-zinc oxide composite for the adsorption of uranium (VI) from aqueous solutions: kinetic and equilibrium profiles," *Materials Today: Proceedings*, vol. 41, p. 557, 2021.

[62] A. Salama, H. A. Aljohani, K. R. Shoueir, and T. Almomani, "Oxidized cellulose reinforced silica gel: new hybrid for dye adsorption," *Materials Letters*, vol. 230, pp. 293–296, 2018.

[63] S. Ben-Ali, I. Jaouali, S. Souissi-Najar, and A. Ouederni, "Characterization and adsorption capacity of raw pomegranate peel biosorbent for copper removal," *Journal of Cleaner Production*, vol. 142, pp. 3809–3821, 2017.

[64] S. Olivera, H. B. Muralidhara, K. Venkatesh, V. K. Guna, K. Gopalakrishna, and K. Y. Kumar, "Potential applications of cellulose and chitosan nanoparticles/composites in wastewater treatment: a review," *Carbohydrate Polymers*, vol. 153, pp. 600–618, 2016.

[65] H. Tsade, B. Abebe, and H. C. Ananda Murthy, "Nano sized Fe–Al oxide mixed with natural maize cob sorbent for lead remediation," *Materials Research Express*, vol. 6, Article ID 085043, 2019.

[66] X. Qinghua, W. Yulu, J. Liqiang, W. Yu, and Q. Menghua, "Adsorption of Cu (II), Pb (II) and Cr (VI) from aqueous solutions using black wattle tannin-immobilized nanocellulose," *Journal of Hazardous Materials*, vol. 339, pp. 91–99, 2017.

[67] H. Yeol, J. Hyuk, Y. Hasegawa et al., "Thiol-functionalized cellulose nano fi ber membranes for the e ff ective adsorption of heavy metal ions in water," *Carbohydrate Polymer*, vol. 234, Article ID 115881, 2020.

[68] N. Elboughdiri, "The use of natural zeolite to remove heavy metals Cu (II), Pb (II) and Cd (II), from industrial wastewater," *Cogent Engineering*, vol. 7, no. 1, Article ID 1782623, 2020.

[69] Z. Mahmood, S. Zahra, M. Iqbal, M. A. Raza, and S. Nasir, "Comparative study of natural and modified biomass of Sargassum sp. for removal of Cd2+ and Zn2+ from wastewater," *Applied Water Science*, vol. 7, no. 7, pp. 3469–3481, 2017.

[70] J. Nyoo, S. Ismadji, and Y. Ju, ""Nanocellulose based biosorbents for wastewater treatment: study of isotherm, kinetic, thermodynamic and reusability," *Environmental Nanotechnology, Monitoring & Management*, vol. 8, no. 43, pp. 134–149, 2017.

[71] K. R. Hall, L. C. Eagleton, A. Acrivos, and T. Vermeulen, "Pore- and solid-diffusion kinetics in fixed-bed adsorption under constant-pattern conditions," *Industrial & Engineering Chemistry Fundamentals*, vol. 5, no. 2, pp. 212–223, 1966.

[72] D. Chauhan and N. Sankararamakrishnan, "Highly enhanced adsorption for decontamination of lead ions from battery wastewaters using chitosan functionalized with xanthate," *Bioresource Technology*, vol. 99, no. 18, pp. 9021–9024, 2008.

[73] Q. Xu, Y. Wang, L. Jin, Y. Wang, and M. Qin, "Adsorption of Cu (II), Pb (II) and Cr (VI) from aqueous solutions using black wattle tannin-immobilized nanocellulose," *Journal of Hazardous Materials*, vol. 339, pp. 91–99, 2017.

[74] M. A. P. Cechinel, S. M. A. G. Ulson de Souza, and A. A. Ulson de Souza, "Study of lead (II) adsorption onto activated carbon originating from cow bone," *Journal of Cleaner Production*, vol. 65, pp. 342–349, 2014.

[75] A. Abdullah, M. Naushad, Z. A. Alothman, and M. Alsuhybani, "Excellent adsorptive performance of a new nanocomposite for removal of toxic Pb (II) from aqueous environment: adsorption mechanism and modeling analysis," *Journal of Hazardous Materials*, vol. 389, Article ID 121896, 2020.

[76] X. Xu, X.-k. Ouyang, and L.-Y. Yang, "Adsorption of Pb(II) from aqueous solutions using crosslinked carboxylated chitosan/carboxylated nanocellulose hydrogel beads," *Journal of Molecular Liquids*, vol. 322, Article ID 114523, 2021.

[77] Y. Zhou, S. Fu, L. Zhang, H. Zhan, and M. V. Levit, "Use of carboxylated cellulose nanofibrils-filled magnetic chitosan hydrogel beads as adsorbents for Pb(II)," *Carbohydrate Polymers*, vol. 101, pp. 75–82, 2014.

[78] R. P. Mohubedu, P. N. E. Diagboya, C. Y. Abasi, E. D. Dikio, and F. Mtunzi, "Magnetic valorization of biomass and biochar of a typical plant nuisance for toxic metals contaminated water treatment," *Journal of Cleaner Production*, vol. 209, pp. 1016–1024, 2019.

[79] R. Md Lutfor, B. Tapan Kumar, M. S. Shaheen et al., "Adsorption of rare earth metals from water using a kenaf cellulose basedpoly(hydroxamic acid) ligand," *Journal of Molecular Liquid*, vol. 243, pp. 616–623, 2017.

[80] L. Chang, W. Qingmiao, F. Jia, and S. Shaoxian, "Adsorption of heavy metals on molybdenum disulfide in water: a critical review," *Journal of Molecular Liquid*, vol. 292, Article ID 111390, 2019.

[81] Z. Chu, P. Zheng, Y. Yu, W. Chaoyang, and Y. Zhuohong, "Compressible nanowood/polymer composite adsorbents for wastewater purification applications," *Composite Science Technology*, vol. 198, Article ID 19810, 2020.

[82] A. Md Ariful, R. P. S. Alain, R. Alejandro et al., "Biomass-derived ultrathin carbon-shell coated iron nanoparticles as high-performance tri-functional HER, ORR and Fenton-like catalysts," *Journal Clean Production*, vol. 275, pp. 124–141, 2020.

[83] C. T. Johnston, S. Wang, and S. L. Hem, "Measuring the surface area of aluminum hydroxide adjuvant," *Journal Of Pharmaceutical Science*, vol. 7, pp. 91–1706, 2002.

[84] I. Langmuir, "The adsorption of gases on plane surfaces of glass, mica and platinum," *Journal of ACS*, vol. 40, no. 9, pp. 1361–1403, 1918.

[85] H. Freundlich, "Uber die Adsorption in Losungen," *Zeitschrift Fur Physical Chemistry*, vol. 57, pp. 385–470, 1906.

[86] M. Temkin, "Kinetics of ammonia synthesis on promoted iron catalysts," *Acta Physiochim URSS*, vol. 12, pp. 327–356, 1940.

[87] T. Fatima Ezzahra, A. Rachid, A. Ali, and H. Mohamed, "Removal of cationic dye from aqueous solution using Moroccan pozzolana as adsorbent: isotherms, kinetic studies, and application on real textile wastewater treatment," *Groundwater Sustainable Development*, vol. 11, Article ID 100405, 2020.

[88] O. Hamdaoui and M. Chiha, "Removal of methylene blue from aqueous solutions by wheat bran," *Acta Chimica Slovenica*, vol. 54, pp. 407–418, 2007.

[89] Y. S. Ho and G. McKay, "Kinetic models for the sorption of dye from aqueous solution by wood," *Process Safety and Environmental Protection*, vol. 76, no. 2, pp. 183–191, 1998.

[90] W. J. Weber and J. C. Morris, "Kinetics of adsorption on carbon from solution," *Journal of the Sanitary Engineering Division*, vol. 89, no. 2, pp. 31–59, 1963.